IOPscience iopscience.iop.org

Home Search Collections Journals About Contact us My IOPscience

Near-surface nanoscale InAs Hall cross sensitivity to localized magnetic and electric fields

This article has been downloaded from IOPscience. Please scroll down to see the full text article.

2009 J. Phys.: Condens. Matter 21 255802

(http://iopscience.iop.org/0953-8984/21/25/255802)

View the table of contents for this issue, or go to the journal homepage for more

Download details:
IP Address: 129.252.86.83
The article was downloaded on 29/05/2010 at 20:14

Please note that terms and conditions apply.

J. Phys.: Condens. Matter **21** (2009) 255802 (9pp) doi:10.1088/0953-8984/21/25/255802

Near-surface nanoscale InAs Hall cross sensitivity to localized magnetic and electric fields

L Folks[1], A S Troup[2], T D Boone[1], J A Katine[1], M Nishioka[1], M Grobis[1], G J Sullivan[3], A Ikhlassi[3], M Field[3] and B A Gurney[1]

[1] Hitachi Global Storage Technologies, San Jose Research Center, 3403 Yerba Buena Road, San Jose, CA 95135, USA
[2] Hitachi Cambridge Laboratory, J J Thomson Avenue, Cambridge CB3 0HE, UK
[3] Teledyne Scientific Company, 1049 Camino Dos Rios, Thousand Oaks, CA 91360, USA

Received 28 February 2009, in final form 11 May 2009
Published 1 June 2009
Online at stacks.iop.org/JPhysCM/21/255802

Abstract
We have measured the room temperature response of nanoscale semiconductor Hall crosses to local applied magnetic fields under various local electric gate conditions using scanning probe microscopy. Near-surface quantum wells of AlSb/InAs/AlSb, located just 5 nm from the heterostructure surface, allow very high sensitivity to localized electric and magnetic fields applied near the device surfaces. The Hall crosses have critical dimensions of 400 and 100 nm, while the mean free path of the carriers is about 160 nm; hence the devices nominally span the transition from diffusive to quasi-ballistic transport. With certain small gate voltages (V_g) the devices of both sizes are strongly responsive to the local magnetic field at the center of the cross, and the results are well described using finite element modeling. At high V_g, the response to local magnetic fields is greatly distorted by strong electric fields applied near the cross corners. However we observe no change in behavior with the size of the device.

1. Introduction

Sub-micrometer Hall crosses have been used to detect magnetic microbeads attached to biochemical markers in biological sensing applications. The technique involves the detection of the small fields from the paramagnetic beads in the presence of a homogeneous background magnetic field used to stabilize the magnetization. Hall cross sensors composed of III–V semiconductor quantum well structures are advantageous since the high carrier concentrations and mobilities that are achievable in these materials greatly enhance the field sensitivity of the sensor [1–4]. It is also critical for biological sensing and similar localized field sensor applications (including scanning Hall probe microscopy [5, 6] or magnetic recording sensors [7, 8]) that the field-sensitive 2DEG be as close to the device surface as possible.

We have explored the room temperature sensitivity of near-surface nanoscale Hall crosses to localized magnetic and electric fields using scanning probe microscopy (SPM) techniques. The Hall crosses have been fabricated with critical dimensions of 100 and 400 nm, as shown in figure 1, from an MBE grown AlSb (2 nm)/InAs (12.5 nm)/AlSb (2 nm) heterostructure in which the top of the InAs two-dimensional electron gas (2DEG) is just 5 nm from the surface. The proximity of the 2DEG to the surface allows high resolution scanning probe microscopy (SPM) of the Hall sensitivity of the crosses to local magnetic and electric fields, applied separately and together.

The work of Eriksson *et al* [9] first showed that an electrically charged scanning probe can be used to alter the local electron density of a 2DEG device and create a local obstruction for electron flow. By scanning the probe across the surface of the device which was held at 4.2 K, Eriksson *et al* were able to image the ballistic current flowing through a point contact in a 2DEG buried ~52 nm below the surface under various gate bias conditions. Baumgartner *et al* [10] followed with low temperature scanning gate experiments on Hall bars of size 4 μm, with the 2DEG again ~52 nm from the surface, and subjected the devices to homogeneous magnetic fields while scanning. The spatial resolution of the scanning gate technique is primarily determined by the depth of the 2DEG from the surface, since this is typically much larger than the probe diameter.

 © 2009 IOP Publishing Ltd Printed in the UK

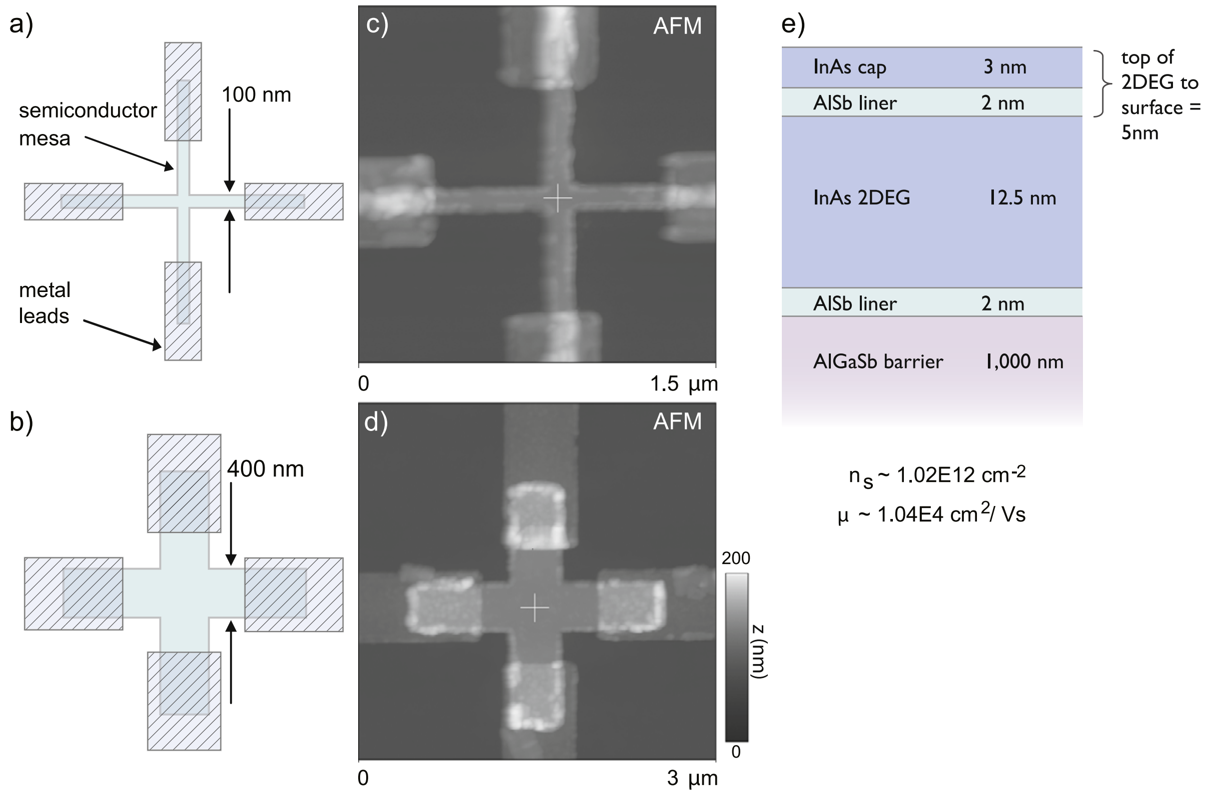

Figure 1. (a) and (b) E-beam mask design for Hall cross devices with critical dimensions of 100 nm and 400 nm respectively, (c) and (d) AFM images of the devices as built, and (e) schematic of the semiconductor structure from which the devices were built.

To reduce the resolution limitation posed by large probe-2DEG separations we have made devices with the top of the 2DEG just 5 nm below the surface, allowing us to perform scanning gate measurements at room temperature with a greatly improved spatial resolution of about 10 nm. In a further step, we have used silicon probes with thin film magnetic coatings, conventionally used for magnetic force microscopy, to map the Hall sensitivity of our devices to local magnetic fields. This approach follows from work by Guillou *et al* [11] and Thiaville *et al* [12] in which (un-gated) magnetized probes were used to map the Hall response to local magnetic fields of large (2 μm) Hall devices fabricated from thick (250 nm) Bi films and a GaAs/AlGaAs 2DEG, respectively. By incorporating a magnetic probe in our scanning gate microscopy experiments, we are able for the first time to manipulate the local electric *and* magnetic fields applied to the nanoscale Hall crosses simultaneously. Further, by using magnetic probe diameters as small as 25 nm and a probe-2DEG separation of $\sim$15 nm, the region over which the magnetic fields extend in the 2DEG is smaller than the sensitive area of the devices. Our method allows the characterization of nanoscale Hall crosses suitable for sensing biomagnetic marker particles on length scales relevant to these applications. This method may be applied also to other planar semiconductor field sensors, such as extraordinary magnetoresistance (EMR) sensors that have potential application as hard disk drive read sensors [8].

Our results in the region of the intersection of the arms of the cross are in good qualitative agreement with a simple diffusive finite element model (FEM) solution of Poisson's equation that incorporates the effect of the Lorentz force through the off-diagonal elements in the conductivity tensor. The effect of the localized extent of the magnetic and electric fields from the probe are approximated in the model by assuming constant fields extending throughout a disk of diameter r of the 2DEG material centered below the probe, where r is determined from the probe diameter and probe to 2DEG spacing. Outside the disk the probe is assumed to have no influence.

The geometry of the model Hall cross structures are assumed to match the lithographic mask, shown in figure 1. The triangular element mesh has been made denser in regions where the potential is expected to change rapidly. In total, the mesh consists of just over 52 000 elements, which ensures sufficient convergence of the solutions. It is assumed that the charge transport is diffusive, and is thus governed by the standard magnetoconductivity tensor in two dimensions. In this expression, the position dependent potential within the Hall cross and the probe are explicitly included:

$$\sigma(V_{\text{disc}}, B_{\text{disc}}) = \frac{ne\mu_{\text{sc}}\left[1 - \{(V_{\text{disc}} - V_{\text{pot}})/V_0\}\right]}{1 + (\mu_{\text{sc}} B_{\text{disc}})^2} \times \begin{bmatrix} 1 & \mu_{\text{sc}} B_{\text{disc}} \\ -\mu_{\text{sc}} B_{\text{disc}} & 1 \end{bmatrix} \quad (1)$$

where V_{pot} is the potential profile in the absence of the SPM probe, which includes the electric potential drop resulting from biasing the cross to induce current flow from the upper to lower

arms of the cross. V_{disc} and B_{disc} are given by:

$$B_{disc}(x,y) = \begin{cases} B_0(x-x_0)^2 + (y-y_0)^2, \\ \quad \text{for } [(x-x_0)^2 + (y-y_0)^2 \leqslant r^2] \\ 0, \ \text{otherwise} \end{cases} \quad (2)$$

$$V_{disc}(x,y) = \begin{cases} V_0(x-x_0)^2 + (y-y_0)^2, \\ \quad \text{for } [(x-x_0)^2 + (y-y_0)^2 \leqslant r^2] \\ 0, \ \text{otherwise} \end{cases} \quad (3)$$

where B_0 and V_0 are the magnitudes of the local magnetic field and locally applied probe potential, within a circle of radius r. The position of the SPM probe is given by (x_0, y_0). The Hall cross material parameters are described by the electron density n and the semiconductor mobility μ_{sc}.

Under steady state conditions, $\nabla\cdot[\sigma\nabla\phi(x,y)] = 0$ where $\phi(x,y)$ is the electrostatic potential at position (x,y). The periphery boundary conditions of the Hall cross structures are set such that $\hat{n}\cdot\boldsymbol{j} = 0$, where $\hat{n}$ is the unit vector perpendicular to the periphery. The boundary conditions for the upper and lower arms are $\hat{n}\cdot\boldsymbol{j} = -I_c/w$ and $\phi = 0$ respectively, where I_c is the applied current and w is the width of the arms. The unbiased arms are set to have floating potentials, such that $\int \hat{n}\cdot\boldsymbol{j} = 0$. The room temperature mobility and carrier concentration used in the model were determined using macroscopic van der Pauw elements lithographically defined near the Hall crosses, and were found to be $\mu = 1 \times 10^4$ cm^2 V^{-1} s^{-1} and $n_s = 1 \times 10^{12}$ cm^{-2}, respectively.

To scale the electric potential of the disk arising from a potential on the probe the following method was used. For a particular experimental result, the potential of the disk in the model, labeled V^* herein, was varied until the resulting modeled Hall voltage image agreed qualitatively with experimental results. The disk potentials for other experimental conditions were then determined by scaling the probe potential. With each probe type (i.e., 5 nm diameter Si probe, or 25 or 80 nm magnetic probe) the method was repeated. Magnetic fields at the 2DEG surface used in the model were estimated from our experience in imaging and reversing magnetic media with such probes, and were taken as being 300 Oe and 600 Oe for the 25 and 80 nm probes, respectively.

2. Experiment and results

The heterostructure used in these experiments was grown by molecular beam epitaxy on an n-type GaAs substrate. In growth order, the layers were; 1 μm $Al_{0.80}Ga_{0.20}Sb$ barrier, 2 nm AlSb liner, 12.5 nm InAs two-dimensional electron gas (2DEG), 2 nm AlSb liner, and 3 nm InAs cap. The top of the 2DEG was thus 5 nm from the surface, as shown in figure 1(e), and is readily perturbed by the local magnetic and electric fields from the probe.

The Hall crosses were fabricated with low resistance ohmic contacts using planar lithography processes. The cross-shaped semiconductor mesas with nominal critical dimensions W of 100 and 400 nm were formed using e-beam lithography and a subtractive 175 V Ar^+ ion mill process. We note that the effective sensor widths may differ from the measured widths since it is known that surface states caused by edge damage during the patterning process can cause charge depletion or accumulation near the edges. The lead and contact structures were defined using e-beam lithography. To create the contacts, an ion mill process was used to remove all the semiconductor material down to just below the lower liner. Subsequently an abutted junction was formed between the metal and the 2DEG using an *in situ* ion beam deposition of 50 Å Ta and 350 Å Au. From measurements of transmission line devices on the same wafer we have found that the specific contact resistivity is below 10^{-7} Ω cm^{-2}, and I–V curves on the Hall crosses show highly ohmic behavior until the onset of impact ionization at about 0.5 V. In homogeneous magnetic fields, these devices show dc field sensitivity of 110–170 V A^{-1} T^{-1} for the 400 nm devices and 130–230 V A^{-1} T^{-1} for 100 nm devices, figures that are comparable with the mesoscopic ($W \sim 2.4$ μm) silicon devices of Besse *et al* [13]. The four point resistance of the 400 nm devices is in the range of 1.2–1.6 kΩ and of the 100 nm devices is in the range of 4–6 kΩ.

Wafer parts were mounted in a chip carrier that allowed for wirebonded contacts to the current and voltage leads of the devices for study. The scanning probe microscopy measurements were undertaken at room temperature in air with a Veeco Dimension 3100 scanning probe microscope with commercially available non-magnetic and magnetic probes (types Veeco TESP, MESP and MESP-HM). Before imaging, care was taken to remove excess charge from the probe using a flowing nitrogen gas blow-off gun incorporating a gold–polonium 210 static eliminator.

In all the data presented here, constant currents are driven across the devices by applying a potential to the upper arm of the cross, while holding the opposing lower arm of the cross at ground. Note that the voltage bias applied to drive the current through the cross, V_{dc}, results in a non-zero voltage at the center of the cross. In a perfectly symmetric device, free of lithographic and material variations and with equal contact resistances, the voltage with respect to ground at the center of the cross is $V_{dc}/2$. It follows that when the gate potential $V_g \sim V_{dc}/2$, the electric field at the center of the Hall cross is close to zero, and we refer to this value as the neutral gate voltage V_{g0}. We note however that experimental factors shift V_{g0} from the ideal value of $V_{dc}/2$, such as differences in current lead contacts, and differences in work function between Hall cross and probe (which may change during imaging if material is collected on the probe or released from it). As a result, we observe experimentally that V_{g0} varies somewhat from device to device, and with measurement conditions, but can nevertheless be determined rather readily by varying V_{dc} around the expected neutral value and noting the value at which the appropriate symmetry changes are observed in the images collected. We expect the local electron density in the 2DEG cross to be a complicated function of the probe (i.e., gate) height above the 2DEG, the probe position relative to the device edges, the probe bias voltage V_g, the device bias current, and possible defects in and at the edges of the semiconductor mesa.

The open circuit Hall voltage is measured between the unbiased arms of the cross (the left and right arms in our

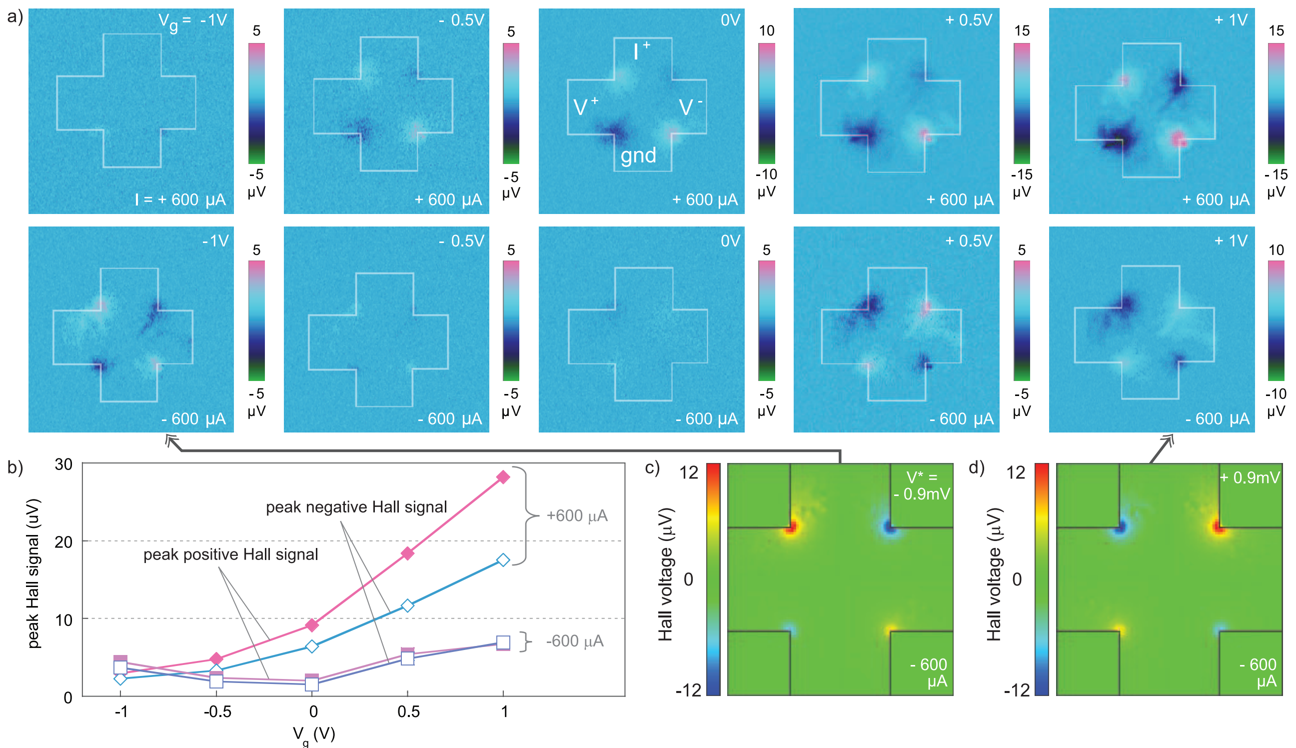

Figure 2. (a) A series of scanning gate images of a 400 nm cross with V_g applied via a non-magnetic probe of diameter ~5 nm, and with forward and reverse current bias. Note that the image z-scales vary in order to show details. (b) Experimental peak signals at the device corners as a function of current bias direction and V_g. Here the positive (negative) peak signal refers to the light (dark) regions in the scanning gate images in (a). (c) and (d) FEM simulation results for a 400 nm cross under conditions approximately matching those for the panels in (a) linked by arrows.

images), and is plotted herein as a function of the x–y location of the probe using a color scale. The Hall voltage is found to be an approximately linear function of the bias current in the devices, with a sensitivity in the 400 nm devices ~0.7 V A^{-1}. An ensemble of scanning gate images of a 400 nm device with different V_g applied via a non-magnetic probe of diameter around 5 nm (Veeco TESP), and with forward and reverse current directions, are shown in figure 2(a) with conditions as labeled in each panel. As may be seen from these images, the scanning gate causes local variations in carrier density and Fermi velocity, and results in changes in the Hall resistance of the device as a function of the position of the probe over the device. As expected from earlier work [10, 14], the scanning gate causes the greatest changes in the Hall voltage when near the device corners, with diagonally opposing corners having the same sign of Hall voltage and adjacent corners the opposite sign. In contrast with earlier experiments, and as a result of improved spatial localization of the gate potential in this experiment, the signal at the center of the cross is zero. Figure 2(b) shows the peak signal strengths from this series of images as a function of V_g. The signal minima occur at different values of V_{g0} for forward and reverse currents as a result of the factors influencing the effective V_{g0} described above. Further, we note that the regions of highest signal are located in the lower half of the cross intersection at positive bias current and switch to the upper half of the cross intersection at negative bias current. This asymmetry is expected from the voltage drop across the cross intersection arising from the bias current flowing through the resistive 2DEG and has been described in earlier modeling [15], although we believe this has not been noted in previous experiments. These observed features are all reproduced in our models, examples of which are given in figures 2(c) and (d) for a 5 nm diameter probe on a 400 nm cross with +600 μA of current and large negative and positive gate potentials, respectively.

A consequence of the near-surface 2DEG used in these devices is the clarity of the fine structure near the corner signal peaks in figure 2(a). We hypothesize that local scattering sites (e.g., impurities or defects) in the device are the source of these features. They vary in structure from device to device, but are always reproducible for a given device, in accord with the low temperature work of Jura *et al* [16].

The same primary features seen in the 400 nm crosses are seen at the corners of the 100 nm crosses in figure 3, namely signal peaks of the same sign on the diagonals that increase in strength nearly linearly with V_g. Again true mirror symmetry along the cross diagonals is broken by the voltage drop across the device caused by the current source, and by local defects within individual devices. The peak signal strength from the 100 nm devices is about 1/3 that obtained from the 400 nm devices, when normalized for bias current density.

We also observe an unexpected feature in our images of 100 nm devices in the form of signal lobes that appear in the *voltage leads* indicating that the local gate is causing a substantial change in the Hall resistance of the device when

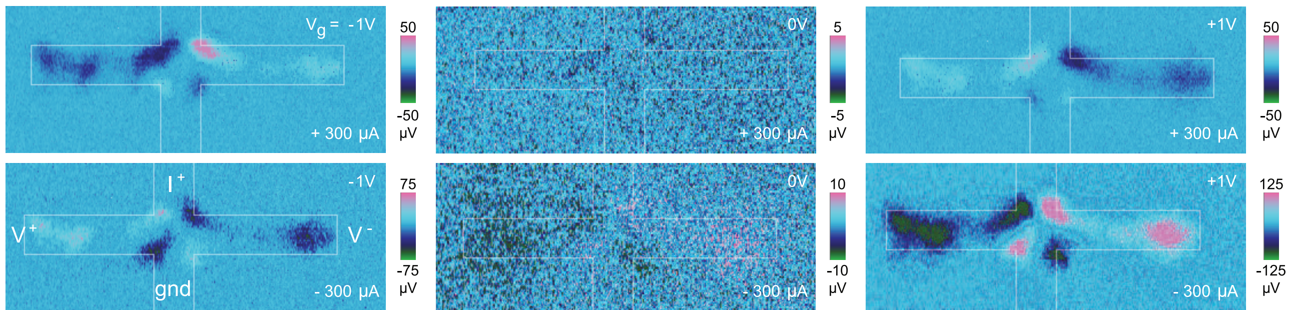

Figure 3. A series of scanning gate images of a 100 nm cross with V_g applied via a non-magnetic probe of diameter ∼5 nm, and with forward and reverse current bias. Note that the image z-scales vary in order to show details.

well away from the intersection of the cross. The effect is observed independent of the choice of leads for Hall resistance measurement, and independent of the physical orientation of the probe used to apply the gate voltage relative to the cross. Reviewing the 400 nm device data in figure 2(a), we note that there is a weak indication of such voltage lead signal lobes at the highest V_g, and it is possible that similar features would be observed if the 400 nm device voltage leads were lengthened by a factor of ∼4 to match the ratio of lead length to cross width of the 100 nm devices. In the diffusive limit, the current is expected to decay quickly in the voltage leads, with an $\exp(-\pi l/W)$ dependence where l is the distance from the current lead and W is the width of the voltage probe. Thus, the Hall voltage signal is expected to saturate quickly, along the voltage leads, approximately in proportion to $(1 - \exp(\pi l/W))$, so that the voltage in the leads far from the cross center should be constant. In the ballistic limit, very few carriers are expected to enter the voltage leads, and so no variation within the voltage leads is expected. In fact, careful analysis of our experimental apparatus leads us to conclude that the origin of the voltage lead signal lobes may be ascribed to an unwanted leakage current passing through the voltage leads. When a highly biased scanning gate passes over the voltage leads, it can completely pinch off the conducting channel in the voltage leads, causing the potential distribution across the whole device to shift resulting in an apparent Hall voltage. (We note that this has apparently been seen before, in the magnetic probe studies of Hall crosses by Thiaville *et al* [12], wherein voltage lead lobes and an elongation of the magnetic response into an oval shape were noted, almost certainly denoting that the probe had residual charge on it (see discussion below), and that there was a leakage current through the voltage leads in that experiment also.)

Magnetic probes of a type conventionally used for magnetic force microscopy studies were used to simultaneously apply local magnetic and electric fields to the devices. Silicon-nitride probes with rather thick (high moment) magnetic thin film coatings, and a probe diameter ∼80 nm (type Veeco MESP-HM), were used in addition to conventional MFM probes with lower moment and diameter ∼25 nm (type Veeco MESP). The magnetic domain configuration in such probes is an ongoing topic of debate, but for the purposes of this work we assume that the probes produce a dipole field that is oriented perpendicular to the surface of the device. While it is not known precisely how much magnetic field these probes produce at the center of the 2DEG layer [12], we can estimate the value based on an understanding of how these probes interact with well-understood magnetic thin films. Observations of domain wall motion and reversal events in, for example, Co/Pt patterned media samples lead us to estimate the field at the 2DEG layer at around 600 ± 50 Oe for the MESP-HM probes and 300 ± 50 Oe for the MESP probes.

In figure 4(a) we show a series of images from a 400 nm device gated with an MESP-HM probe in which V_g, the probe magnetization direction (i.e., up or down, relative to the sample surface plane), and the bias current direction are varied as noted in each panel. Here the primary feature is a large signal peak at the center of the cross, as expected from modeling work [15].

The peak elongates across the cross diagonals when V_g is increased away from V_{g0}, with a change in the orientation of the signal structure with the sign of V_{g0}–V_g. The Hall voltage signal also changes sign when the current polarity is reversed, and when the magnetization direction changes, as expected from prior models. The signal magnitude is between 5 and 10 times larger with the magnetic probe compared with the non-magnetic (but much smaller diameter) probe, and the purely capacitive gating effects seen in figure 2(a) at the device corners are difficult to detect by eye in figure 4(a). These effects are readily modeled, and an example of our FEM output is shown in figure 4(b), corresponding to the panel linked with an arrow. The subtle asymmetry in peak strength attributable to the voltage drop across the center of the device due to the bias current source is illustrated in figure 4(c), a series of cross sections from the data set in figure 4(b), wherein the negative peak at +200 nm is of greater magnitude by a few per cent than the negative peak at −200 nm.

The plot in figure 4(d) shows that there is a local maximum in the peak signal at small negative V_g, and that peak signal strength increases with increasing V_g away from this region. The highest signal is observed with negative current bias and the probe magnetized down, however, the signal strength changes by only ∼10% in this entire series of images, in contrast with the strong changes in signal strength as a function of V_g observed with the non-magnetic probe (figures 2 and 3). That is, within this range of experimental parameters, the device response is dominated by the effect of the probe's *magnetic* field on the electron transport in the 2DEG; the gating affects the *shape* of the sensitive region, but not significantly

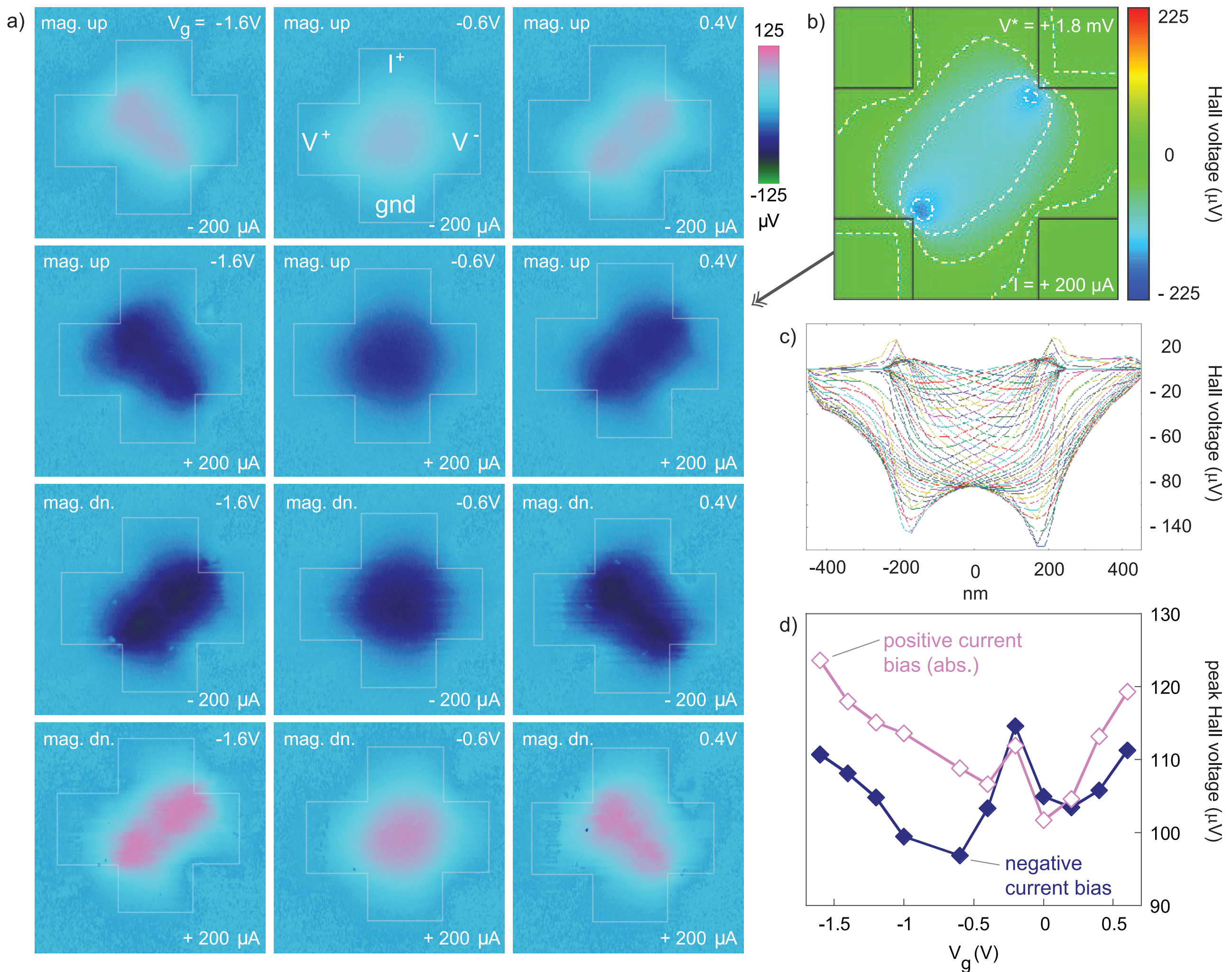

Figure 4. (a) A series of images of a 400 nm cross collected with a high moment magnetic probe of diameter ∼80 nm. In addition to varying V_g and the bias current direction, the orientation of the magnetization of the probe has been changed from 'up' to 'down', relative to the device surface, as indicated in each panel. The Hall voltage z-scales of all images are the same. (b) FEM simulation result for a 400 nm cross under conditions matching those for the second-from-top right image in (a). (c) Series of cross sections through the FEM result in (b), showing asymmetry in the left and right negative peaks due to bias current source. (d) Peak signal values from the 'mag. up' images in (a) as a function of V_g, showing a minor peak near V_{g0}.

the signal magnitude. The measured local magnetic field sensitivity at V_{g0} ∼ 10 V A^{-1} T^{-1} is significantly smaller (at 6–9%) than the homogeneous magnetic field sensitivity range of 110–170 V A^{-1} T^{-1} measured using a conventional probe station. Such a reduction to is to be expected from purely geometric considerations if the assumption that signal is proportional to the average magnetic flux cutting the Hall cross holds [12], from which we would expect a reduction to around 4% of the homogeneous field sensitivity in the local magnetic field case. These results are qualitatively similar to those in [10] for a homogeneous magnetic field.

In figure 5 we present a series of FEM images, with model conditions as noted on the panels, that qualitatively reproduce the key features of the data in figure 4. From these images the effective splitting of the centered, circular, magnetic response region observed with low V_g into the broadly spaced pair of peaks along the cross diagonals observed with high V_g is strikingly shown.

Applying such a large V_g to a high moment magnetic probe while scanning a 400 nm device indeed causes the magnetic signal to elongate strongly along the cross diagonal, splitting into two peaks, as seen in the dark (negative) signal regions in the images in figure 6. In addition, the capacitive effects of the strong gate potential are now seen in the appearance of the two positive (pink) signal lobes in the corners away from the magnetic peaks. Under these conditions, the signal obtained from electric and magnetic field excitation are approximately equal, in strong contrast with the images in figure 4(a) obtained with low V_g.

Results for measurements with an MESP-HM probe on a 100 nm cross are shown in figure 7. The same features seen in the center of the cross as for the 400 nm devices are observed, namely a central peak that elongates along the diagonal axis with increasing V_g, and which changes in sign when the current or magnetic field directions are reversed. Again, the peak signal strength varies only by ∼10% over the range of V_g

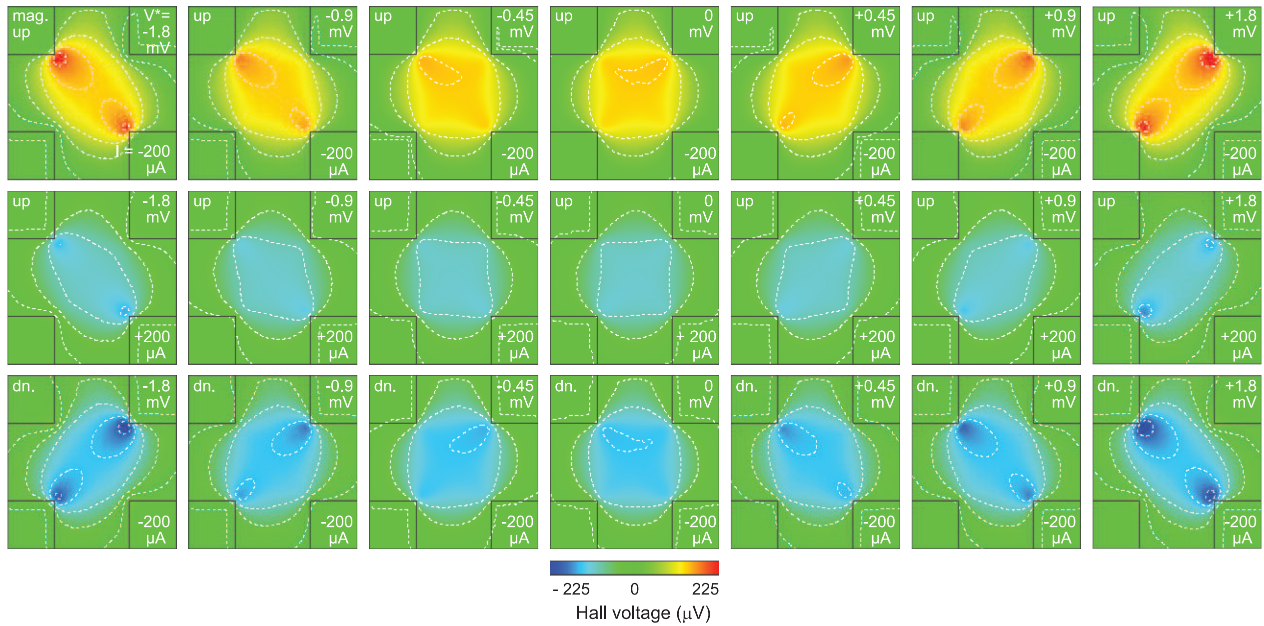

Figure 5. Series of FEM simulation images showing the evolution of the Hall response in a 400 nm cross as a function of varying currents and gate potentials, with conditions as indicated in each panel. The electric potential of the disk arising from the potential on the probe, V^*, has been used to scale the images to give qualitative agreement with the experimental data.

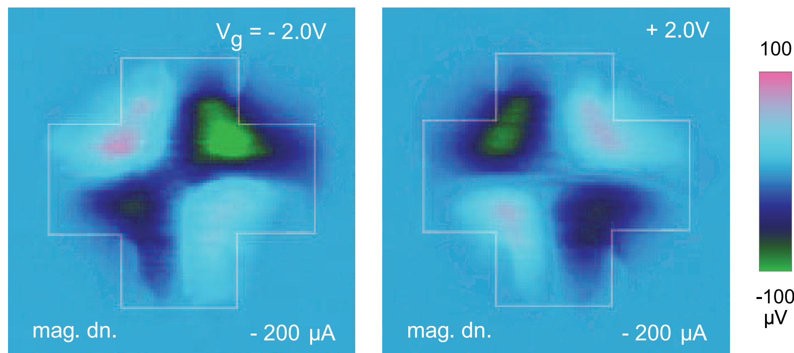

Figure 6. Scanning gate images with an MESP-HM probe from a 400 nm cross with large positive (left) and large negative (right) V_g, showing the splitting of the magnetic signal (here dark/negative) into two peaks, and the influence of the electric field apparent in the two light/positive peaks at the opposing corners.

explored here, as for the 400 nm devices. In the 100 nm devices however we obtain around three times *more* signal than from the 400 nm devices, after normalizing for constant current density. Further, the peak local magnetic field sensitivity at V_{g0} is $\sim$25 V A^{-1} T^{-1} as compared with homogeneous magnetic field sensitivity range for the 100 nm devices of 130–230 V A^{-1} T^{-1}. That is, with a probe of diameter now approaching the critical dimension of the device, the local magnetic field sensitivity is less than one order of magnitude lower than the homogeneous field sensitivity, as might be expected from purely geometric considerations. (Note too that, while less fine detail is seen in figure 7 than in figure 3, the voltage lead signal lobes caused by leakage currents are present again with high V_g.)

More detailed information can be obtained by using a smaller magnetic probe to improve the spatial resolution of the data. In figure 8 we show data collected from a 100 nm cross using a standard MFM probe (Veeco MESP), with a probe diameter around 25 nm and around half the magnetic moment of the MESP-HM probes. Using the smaller probe reduces the peak Hall voltage signal by $\sim$5% for the same imaging conditions. Recall however that the change in probe diameter dramatically affects the field distributions at the 2DEG for the same V_g, and this increased localization of the fields apparently largely compensates for the decrease in moment of the probe.

It is notable that in figure 8, collected with a probe of diameter $\sim$25 nm, there is far greater fine detail resolved than with broad, high moment probe of figure 7. The local magnetic field sensitivity is $\sim$21 V A^{-1} T^{-1}, i.e., to a good approximation the local field sensitivity is the same for the high moment and the regular MFM probes. Also, for both types of magnetic probe we see the broken x–y symmetry (diagonally opposite signal peaks are not of the same magnitude) arising from the choice of current leads, as was observed with the non-magnetic probes, and in agreement with our diffusive model results and previous model work [15].

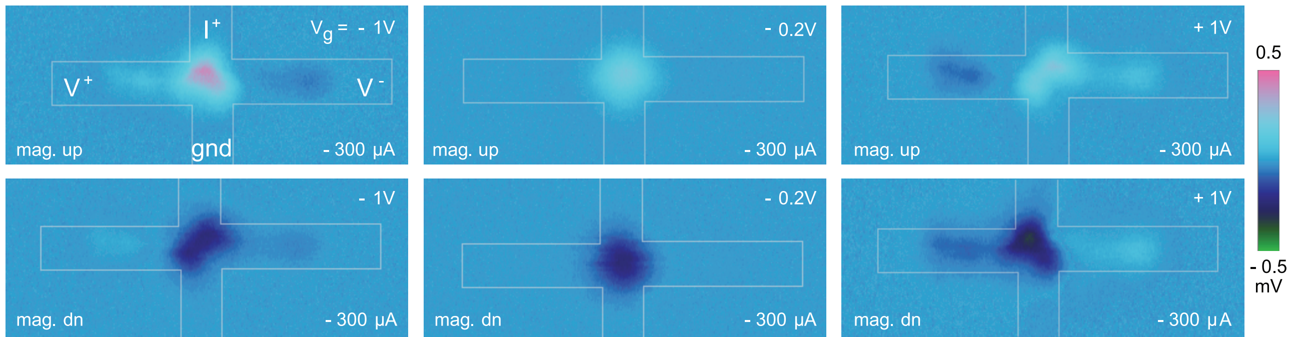

Figure 7. A series of scanning gate images of a 100 nm cross collected with a high moment magnetic probe of diameter ~80 nm, and with constant current bias of $-300\ \mu$A. The values of V_g and the orientation of the magnetization of the probe are indicated in each panel.

Figure 8. A series of scanning gate images of a 100 nm cross collected with a regular MFM magnetic probe of diameter ~25 nm. The values of V_g, bias current, and the orientation of the magnetization of the probe are indicated in each panel.

3. Discussion

Reflecting the potential of using Hall crosses to detect local nanoscale electric and magnetic field sensors, there have been a number of substantial modeling efforts to understand diffusive transport [15, 17] and ballistic transport [18, 19] with inhomogeneous magnetic fields in the past decade. The diffusive model of Ibrahim *et al* [18] predicts a single peak

signal at the center of the Hall cross when a large magnetic-moment dot of radius $r_o = W/3$ is scanned across the device. In that work, the sensitive region of the Hall cross was found to be nearly $2W$, while in our 400 nm device results (see figure 4), $r_o \sim W/10$ and the sensitive region has FWHM $\sim 3W/2$, which is comparable.

The most prominent spatial features of the Hall resistance signals we obtain are the same for our large (400 nm) and small (100 nm) devices: (a) local electric potentials result in peaks at each of the corners of the devices that change sign with current bias direction and with a change in the sign of the local gate potential, and (b) local magnetic potentials result in centered peaks in the Hall cross intersection that elongate along the cross diagonals when large gate voltages are applied. These results are consistent with diffusive modeling of transport in Hall crosses generated by us and by others [14].

In conclusion, we have made the first measurements of the room temperature response of semiconductor Hall crosses to local applied magnetic fields under various local gate conditions. Key to this result was the use of 400 and 100 nm Hall crosses built from high mobility near-surface AlSb/InAs/AlSb 2DEGs. Although we built devices that nominally span the diffusive/quasi-ballistic transport transition, we observe the same key features within the cross regions in the small (100 nm) and large (400 nm) devices excited by local electric and magnetic fields. The use of probes of differing diameters has allowed the influence of the spatial extent of the local field sources, as a fraction of the device dimension, on signal form and strength to be quantified and compared with model data. Fine structure within the Hall voltage maps is attributed to local scattering sites within the heterostructure, and these are mapped with a spatial resolution of around 10 nm. The data demonstrate the importance of optimizing device electric gate conditions for maximizing magnetic field sensitivity at the center of the cross if the Hall cross is to be used as a local magnetic field sensor [20], for example in biomarker detection or magnetic recording sensor applications.

References

[1] Boero G, Demierre M, Besse P-A and Popovic R S 2003 Micro-Hall devices: performance, technologies and applications *Sensors Actuators* A **106** 314–20
[2] Sandhu A and Handa H 2005 Practical Hall sensors for biomedical instrumentation *IEEE Trans. Magn.* **41** 4123
[3] Mihajlovic G, Aledealat K, Xiong P, von Molnar S, Field M and Sullivan G J 2007 Magnetic characterization of a single superparamagnetic bead by phase-sensitive micro-Hall magnetometry *Appl. Phys. Lett.* **91** 172518
[4] Mihajlovic G, Xiong P, von Molnar S, Field M and Sullivan G J 2007 InAs quantum well devices for room-temperature detection of single biomolecular labels *J. Appl. Phys.* **102** 034506
[5] Chang A M, Hallen H D, Harriott L, Hess H F, Kao H L, Kwo J, Miller R E, Wolfe R, van der Ziel J and Chang T Y 1992 Scanning Hall probe microscopy *Appl. Phys. Lett.* **61** 1974
[6] Oral A, Bending S J and Henini M 1996 Real-time scanning Hall probe microscopy *Appl. Phys. Lett.* **69** 1324
[7] Solin S, Hines D R, Rowe A C H, Tsai J S, Pashkin Y A, Chung S J, Goel N and Santos M B 2002 Nonmagnetic semiconductors as read-head sensors for ultra-high-density magnetic recording *Appl. Phys. Lett.* **80** 4012
[8] Boone T D, Smith N, Folks L, Katine J A, Marinero E E and Gurney B A 2009 Mesoscopic EMR device magnetic sensitivity in I-V-I-V configuration *IEEE Electron Device Lett.* **30** 117
[9] Eriksson M A, Beck R G, Topinka M, Katine J A, Westervelt R M, Campman K L and Gossard A C 1996 Cryogenic scanning probe characterization of semiconductor nanostructures *Appl. Phys. Lett.* **69** 671
[10] Baumgartner A, Ihn T, Ensslin K, Papp G, Peeters F, Maranowski K and Gossard A C 2006 Classical Hall effect in scanning gate experiments *Phys. Rev.* B **74** 165426
[11] Guillou H, Kent A D, Stupian G W and Leung M S 2003 Geometries for high spatial resolution Hall probes *J. Appl. Phys.* **93** 2746
[12] Thiaville A, Belliard L, Majar D, Zeldov E and Miltat J 1997 Measurement of the stray field emanating from magnetic force microscope tips by Hall effect microsensors *J. Appl. Phys.* **82** 3182
[13] Besse P-A, Boero G, Demierre M, Pott V and Popovic R 2002 Detection of a single magnetic microbead using a miniaturized silicon Hall sensor *Appl. Phys. Lett.* **80** 4199
[14] Papp G and Peeters F M 2007 Resistance maps for a submicron Hall electrosensor in the diffusive regime *J. Appl. Phys.* **101** 113717
[15] Cornelissens Y G and Peeters F M 2002 Response function of a Hall magnetosensor in the diffusive regime *J. Appl. Phys.* **92** 2006
[16] Jura M P, Topinka M A, Urban L, Yazdani A, Shtrikman H, Pfeiffer L N, West K W and Goldhaber-Gordon D 2007 Unexpected features of branched flow through high-mobility two-dimensional electron gases *Nat. Phys.* **3** 841
[17] Bending S J and Oral A 1997 Hall effect in a highly inhomogeneous magnetic field distribution *J. Appl. Phys.* **81** 3721
[18] Ibrahim S, Schweigert V A and Peeters F M 1998 Diffusive transport in a Hall junction with a microinhomogeneous magnetic field *Phys. Rev.* B **57** 15416
[19] Peeters F M and Li X Q 1998 Hall magnetometer in the ballistic regime *Appl. Phys. Lett.* **72** 572
[20] Hicks C W, Luan L, Moler K A, Zeldov E and Shtrikman H 2007 Noise characteristics of 100 nm scale GaAs/Al_xGa_{1-x}As scanning Hall probes *Appl. Phys. Lett.* **90** 133512